AIAA SciTech
4-8 January 2016, San Diego, California, USA
54th AIAA Aerospace Sciences Meeting

CrossMark
click for updates

On the Symmetrization in POD-Galerkin Model for Linearized Compressible Flows

Mehdi Tabandeh*, Mingjun Wei†
New Mexico State University, Las Cruces, NM 88003
James P. Collins
Army Research Laboratory, Aberdeen Proving Grands, MD 21005

Downloaded by Mingjun Wei on February 5, 2016 | http://arc.aiaa.org | DOI: 10.2514/6.2016-1106

Reduced-order models (ROM) based on POD-Galerkin projection have shown success in many problems since the approach was introduced approximately two decades ago. Traditionally, the inner product used in computation is L^2 type to represent kinetic energy. In this paper, our work focuses on the comparison of L^2 inner product and the symmetry inner product introduced by Barone and co-authors (2008). The numerical simulation and analysis are based on a linear acoustic problem controlled by the linearized Euler equation, which, without viscosity, is more sensitive to instability than the Navier-Stokes equation. In our study, besides the stability advantage noticed by Barone's group, much better accuracy and convergency are also shown in the ROM using symmetry inner product. In the test case, symmetry inner product allows to use only 8 modes for the model results to match the exact solution, while L^2 inner product requires 16 modes for similar convergency. The dynamic behavior described by phase portraits of mode coefficients also gives a cleaner picture when symmetry inner product is used.

Nomenclature

$\mathbf{U}$	Instantaneous snapshots or state vector
$\boldsymbol{\phi}$	POD basis
x	Space coordinate
$\mathcal{N}$	Governing equation operator
$\mathcal{L}$	Linear part of governing equation operator
$\mathcal{N}_2$	Quadratic nonlinear part of governing equation operator
$\mathcal{N}_3$	Cubic nonlinear part of governing equation operator
$\mathbf{H}$	Symmetrized matrix
$\mathbf{L}$	Linear ROM coefficient matrix
a_j	temporal coeficients
$\boldsymbol{A}$	Coefficient matrix for linearized Euler equation

I. Introduction

High-fidelity numerical simulations of complex systems are often expensive despite the breathtaking advances in computers in recent years. For many applications, reduced-order model (ROM) becomes attractive for its fast computation with reasonable accuracy. The development and application of ROM have been seen in many different research areas with different approaches [1–13].

Model order reduction, as a way to construct ROMs, is to reduce the complexity of a system from its original number of degree of freedom (e.g. large number of mesh points in direct numerical simulation) to a much lower order (e.g. a couple of base functions/modes). POD-Galerkin projection, since its introduction

*Research Assistant, Department of Mechanical and Aerospace Engineering
†Associate Professor, Department of Mechanical and Aerospace Engineering, Associate Fellow AIAA

This material is declared a work of the U.S. Government and is not subject to copyright protection in the United States.

to fluid mechanics [14, 15], has become one of the most popular approaches for model order reduction. Proper orthogonal decomposition (POD) provides orthogonal bases which represent the given ensemble of data in a well-defined least-square optimum. Galerkin projection is then used to project the original system to a subspace with limited number of these optimal bases to construct a low-order approximate system. Usually, the same inner product, which defines a Hilbert space, is used in both POD and Galerkin projection processes, though there have been exceptions [10]. An L^2 norm representing kinetic energy provides a common choice for inner product. However, it is not always the best choice [9,16]. Since symmetrization has shown the advantage to make incompletely parabolic equations well-posed and provide stable solutions [17], it is promising to apply the same principle on model order reduction to improve ROMs. Barone et. al [18] adopted the idea of symmetrization along with boundary treatments to construct a symmetry ROM system which shows better stability in comparison to a ROM using traditional L^2 type of inner product. In the current work, we applied the symmetrization on the same linearized Euler equation, but extended the study further to understand its effect not only on stability but also on convergency (with the number of modes) and accuracy.

The remainder of this paper is organized as follows. In section II, basics of POD and Galerkin projection are briefly reviewed. In section III, there is detailed derivation of ROMs for the linearized Euler equations. Both L^2 and symmetry inner product are used in derivation. The results from ROMs derived with different inner products are shown in section IV, where analyses on stability, convergency, and accuracy are also taken. Finally, the conclusion is in section V.

Downloaded by Mingjun Wei on February 5, 2016 | http://arc.aiaa.org | DOI: 10.2514/6.2016-1106

II. Basics on POD and Galerkin Projection

II.A. POD

An inner product space is a vector space which associates each pair of vectors in the space with a scalar known as the inner product. These spaces provide the means of defining the orthogonality between vectors with zero inner product. An inner product generates a norm, thus its space is a normed vector space.

Consider an ensemble of instantaneous snapshots $\left\{\mathbf{U}^k\left(\mathbf{x}\right)|k=1,\ldots,m\right\}$ of real vector solution fields on the domain $\mathbf{x}\in\Omega$. The field can be a set of analytical, experimental, or numerical simulation data. The $\mathbf{U}$'s are assumed to belong to a Hilbert space $\mathcal{H}(\Omega)$ with associated inner product $\langle\mathbf{V},\mathbf{W}\rangle$, where $\mathbf{V}$ and $\mathbf{W}$ are the arbitary vectors. The goal is to find the optimal and orthogonal linear bases to describe the data by its linear combination

$$\mathbf{U}\left(\mathbf{x},t\right)=\sum_{j=0}^{n}a_j(t)\boldsymbol{\phi}_j\left(\boldsymbol{x}\right), \tag{1}$$

with $\boldsymbol{\phi}_j$'s being the bases. The *optimality* here can be defined by the minimization of the average error between the original snapshot data and the reconstruction from the subspace with limited number of bases. POD modes are defined by the fact that the averaged projection of the ensemble $\mathbf{U}^k$ onto $\boldsymbol{\phi}$ should be a maximum. This optimization problem leads to an eigenvalue problem as follows

$$\mathbf{R}\boldsymbol{\phi}=\lambda\boldsymbol{\phi}, \tag{2}$$

where $\mathbf{R}$ is the spatial autocorrelation tensor for the flow field. The method of snapshots [19] allows the correlation to be changed to between snapshots in time sequence and usually brings down the computational cost to compute POD from numerical simulation data.

II.B. Galerkin Projection

In the process of Gelerkin projection, the above linear combination with POD bases in (1) is substituted into the original governing equation denoted by an arbitrary linear or nonlinear operator $\mathcal{N}$, and the equation is then projected on the subspace spanned by the same bases,

$$\langle\mathcal{N}\left[\mathbf{U}(\mathbf{x},t)\right],\boldsymbol{\phi}_i\rangle=0. \tag{3}$$

The operator $\mathcal{N}$ in a generic nonlinear equation can be assumed a form,

$$\mathcal{N}\left[\mathbf{U}(\mathbf{x},t)\right]=\frac{\partial\mathbf{U}}{\partial t}-\mathcal{L}\mathbf{U}-\mathcal{N}_2\left(\mathbf{U},\mathbf{U}\right)-\mathcal{N}_3\left(\mathbf{U},\mathbf{U},\mathbf{U}\right)=\mathbf{0}, \tag{4}$$

where $\mathcal{L}$ is the linear operator, $\mathcal{N}_2$ and $\mathcal{N}_3$ are the quadratic and cubic nonlinear operators respectively. The projection of (4) leads to

$$\left\langle \frac{\partial \mathbf{U}}{\partial t}, \boldsymbol{\phi}_i \right\rangle = \langle \mathcal{L}\mathbf{U}, \boldsymbol{\phi}_i \rangle + \langle \mathcal{N}_2 (\mathbf{U}, \mathbf{U}), \boldsymbol{\phi}_i \rangle + \langle \mathcal{N}_3 (\mathbf{U}, \mathbf{U}, \mathbf{U}), \boldsymbol{\phi}_i \rangle = 0. \tag{5}$$

Expanding $\mathbf{U}$ by its POD modes in (5), with the simplification by orthogonality, the original PDE becomes an ODE of mode coefficients:

$$\begin{aligned} \dot{a}_i = & \sum_{j=0}^{N} a_j \left\langle \boldsymbol{\phi}_i, \mathcal{L}(\boldsymbol{\phi}_j) \right\rangle + \sum_{j=0}^{N} \sum_{k=0}^{N} a_j a_k \left\langle \mathcal{N}_2(\boldsymbol{\phi}_j, \boldsymbol{\phi}_k), \boldsymbol{\phi}_i \right\rangle + \\ & + \sum_{j=0}^{N} \sum_{k=0}^{N} \sum_{l=0}^{N} a_j a_k a_l \left\langle \mathcal{N}_3(\boldsymbol{\phi}_j, \boldsymbol{\phi}_k, \boldsymbol{\phi}_l), \boldsymbol{\phi}_i \right\rangle . \end{aligned} \tag{6}$$

The truncation of number of modes in N leads to a model with lower order at N, when N is much smaller than the original degree of freedom (e.g. number of mesh points).

III. Reduced Order Model for Linearized Euler Equations

In this work, we considered the same one-dimensional linearized Euler equation as it was used by Barone et. al [18]:

$$\frac{\partial \mathbf{U}}{\partial t} + \mathbf{A} \frac{\partial \mathbf{U}}{\partial x} = \mathbf{0}, \tag{7}$$

where $\mathbf{U}$ is the time-varying state vector,

$$\mathbf{U} = \begin{bmatrix} u \\ \xi \\ p \end{bmatrix}, \tag{8}$$

which fluctuats around a steady uniform mean flow $\bar{\mathbf{U}} = [\, \bar{u} \quad \bar{\xi} \quad \bar{p} \,]^T$, and

$$\mathbf{A} = \begin{bmatrix} \bar{u} & 0 & \bar{\xi} \\ -\bar{\xi} & \bar{u} & 0 \\ \gamma \bar{p} & 0 & \bar{u} \end{bmatrix}, \tag{9}$$

with u, ξ, and p being the flow velocity, specific volume, and pressure, $\bar{u}$, $\bar{\xi}$, and $\bar{p}$ being the mean values, and γ the heat capacity ratio.

A one-dimensional acoustic pulse defined below as the initial condition,

$$u = \exp(-(x - x_0)^2), \quad p = \bar{\rho}\bar{c}u, \quad \frac{\rho}{\bar{\rho}} = -\left(\frac{p}{\bar{p}}\right)^{\frac{1}{\gamma}}. \tag{10}$$

Instead of using numerical solution [18], we resort to get an analytical solution and develop the ROM from snapshots of the analytical solutions. The exact solution used here avoids possible numerical perturbation and further assure the accuracy of stability analysis, which was suggested to be subtle in the same work by Barone et. al [18]. The exact solutions are

$$u(x,t) = \exp\left[-(x - x_0 - (\bar{u} + \bar{c})t)^2\right], \tag{11}$$

$$p(x,t) = \bar{\rho}\bar{c} \exp\left[-(x - x_0 - (\bar{u} + \bar{c})t)^2\right], \tag{12}$$

$$\begin{aligned} \xi(x,t) \quad = \quad & \frac{\bar{\xi}}{\bar{c}} \left\{ \exp\left[-(x - x_0 - \bar{u}t)^2\right] - \exp\left[-(x - x_0 - (\bar{u} + \bar{c})t)^2\right] \right\} \\ & + \bar{\xi} \frac{\left[\frac{\gamma}{\bar{c}} \exp\left(-(x - x_0 - \bar{u}t)^2\right)\right]^{\frac{1}{\gamma}}}{1 + \left[\frac{\gamma}{\bar{c}} \exp\left(-(x - x_0 - \bar{u}t)^2\right)\right]^{\frac{1}{\gamma}}}, \end{aligned} \tag{13}$$

Downloaded by Mingjun Wei on February 5, 2016 | http://arc.aiaa.org | DOI: 10.2514/6.2016-1106

where $\bar{c}$ is the mean speed of sound.

These solutions cannot be readily separated into temporal and spatial basis functions. Therefore, we first computed the solution at different time moments (e.g. snapshots) from the exact solution, then used the method of snapshots to compute the POD modes, last constructed the Galerkin system with the POD modes [20]. Note that different boundary conditions can be applied for a domain at $0 \leq x \leq L_x$. The solution was performed over a non-dimensional total time T_{tot} with a uniform time interval dt. Let an ensemble of M snapshots be given at the discrete times t_m,

$$\mathbf{U}^{(m)}(x) = \mathbf{U}(x, t_m). \tag{14}$$

The discrete form of the correlation function is a matrix $\mathbf{C}$, which in index notation reads

$$\mathbf{C}_{mn} := \frac{1}{M} \langle \mathbf{U}(x, t_m), \mathbf{U}(x, t_n) \rangle_\Omega, \tag{15}$$

where $m, n = 1, \cdots, M$. The following eigen problem needs to be solved

$$\mathbf{C}\mathbf{a}^{[i]} = \lambda_i \mathbf{a}^{[i]}. \tag{16}$$

Then the eigenvectors of the correlation matrix are the temporal coefficients $\mathbf{a}^{[i]} = \left(a_1^{[i]}, \cdots, a_M^{[i]}\right)$. The symmetry of $\mathbf{C}$ indicates non-negative eigenvalues and the orthogonality of the eigenvectors. Based on the orthogonality, the POD modes are computed by

$$\mathbf{U}_i = \frac{1}{M\lambda_i} \sum_{m=1}^{M} a_m^{[i]} \mathbf{U}^{(m)}. \tag{17}$$

The second step for constructing the reduced order model is to project the governing PDE onto the POD bases. The linear PDE reads

$$\frac{\partial \mathbf{U}}{\partial t} = \mathcal{L}\mathbf{U}, \tag{18}$$

where $\mathcal{L}$ is the linear operator, $(-\mathbf{A} \cdot \nabla)$, in aforementioned linearized Euler equation (7). The Galerkin projection of (18) onto each POD mode ϕ_i is

$$\left\langle \frac{\partial \mathbf{U}}{\partial t}, \phi_i \right\rangle = \langle \mathcal{L}\mathbf{U}, \phi_i \rangle. \tag{19}$$

Substituting the POD decomposition of $\mathbf{U}$ into (19), and applying the algebraic rules of inner products along with orthogonality of the POD basis yields an ODE,

$$\dot{a}_i = \sum_j a_j \langle \phi_i, \mathcal{L}(\phi_j) \rangle, \tag{20}$$

which is the reduced order model of (18). This time-dependent system of ODE's has the order of the number of retained POD modes M, with $i = 1, \cdots, M$. The inner products in (20) are functionals of the POD modes $\phi(x)$, which are time-independent. These inner products make the ROM coefficient matrix and may be precomputed before the integration of the ROM.

To calculate the inner product, $l_{ij} = \langle \phi_i, \mathcal{L}(\phi_j) \rangle$ in (20), one needs to specify the definition of inner product. Different inner product, L^2 or symmetry inner products, leads to different derivations and equations from this point:

- **L^2 inner product**

  For two arbitrary vectors, $\mathbf{U}^{(1)}$ and $\mathbf{U}^{(2)}$, the L^2 inner product is defined for the current variables as

$$\left\langle \mathbf{U}^{(1)}, \mathbf{U}^{(2)} \right\rangle_{L^2} = \int_\Omega \left[u^{(1)} u^{(2)} + \xi^{(1)} \xi^{(2)} + p^{(1)} p^{(2)} \right] d\Omega. \tag{21}$$

  For this inner product, and with a modal basis $\mathbf{U}_M = \sum_{i=1}^{M} a_i(t) \boldsymbol{\phi}_i(x)$ with

$$\boldsymbol{\phi}_i = \begin{bmatrix} \phi_i^{(1)} \\ \phi_i^{(2)} \\ \phi_i^{(3)} \end{bmatrix}, \tag{22}$$

Downloaded by Mingjun Wei on February 5, 2016 | http://arc.aiaa.org | DOI: 10.2514/6.2016-1106

the ROM coefficient matrix, L, is defined by its entries l_{ij},

$$\begin{aligned} l_{ij} &= -\int_\Omega \left[\bar{u}\phi_i^{(1)} \frac{\partial \phi_j^{(1)}}{\partial x} + \bar{\xi}\phi_i^{(1)} \frac{\partial \phi_j^{(3)}}{\partial x} - \bar{\xi}\phi_i^{(2)} \frac{\partial \phi_j^{(1)}}{\partial x} \right. \\ &\quad \left. + \bar{u}\phi_i^{(2)} \frac{\partial \phi_j^{(2)}}{\partial x} + \gamma\bar{p}\phi_i^{(3)} \frac{\partial \phi_j^{(1)}}{\partial x} + \bar{u}\phi_i^{(3)} \frac{\partial \phi_j^{(3)}}{\partial x} \right] d\Omega. \end{aligned} \tag{23}$$

- **Symmetry inner product**

Following the derivation of Gustafsson [17] for symmetrization of the linearized Euler equations, the definition of symmetry inner product for two arbitrary vectors, $\mathbf{U}^{(1)}$ and $\mathbf{U}^{(2)}$, is

$$\begin{aligned} \left\langle \mathbf{U}^{(1)}, \mathbf{U}^{(2)} \right\rangle_H &= \int_\Omega \left[\bar{\rho} \left(u^{(1)} u^{(2)} \right) + \alpha^2 \gamma \bar{p} \bar{\rho}^2 \xi^{(1)} \xi^{(2)} \right. \\ &\quad \left. + \frac{1+\alpha^2}{\gamma\bar{p}} p^{(1)} p^{(2)} + \alpha^2 \bar{\rho} \left(\xi^{(1)} p^{(2)} + p^{(1)} \xi^{(2)} \right) \right] d\Omega. \end{aligned} \tag{24}$$

The symmetrizing matrix $\mathbf{H}$ is used to define the symmetry inner product:

$$\mathbf{H} = \begin{bmatrix} \bar{\rho} & 0 & 0 \\ 0 & \alpha^2 \gamma \bar{p} \bar{\rho}^2 & \bar{\rho}\alpha^2 \\ 0 & \bar{\rho}\alpha^2 & \frac{1+\alpha^2}{\gamma\bar{p}} \end{bmatrix}, \tag{25}$$

where α^2 is an arbitrary real nonzero parameter. The ROM coefficient matrix, L, is accordingly defined by

$$\begin{aligned} l_{ij} &= -\int_\Omega \left[\bar{\rho}\bar{u}\phi_i^{(1)} \frac{\partial \phi_j^{(1)}}{\partial x} + \phi_i^{(1)} \frac{\partial \phi_j^{(3)}}{\partial x} + \phi_i^{(3)} \frac{\partial \phi_j^{(1)}}{\partial x} + \alpha^2 \bar{\rho}\bar{u}\gamma\bar{p}\phi_i^{(2)} \frac{\partial \phi_j^{(2)}}{\partial x} \right. \\ &\quad \left. + \alpha^2 \bar{\rho}\bar{u} \left(\phi_i^{(2)} \frac{\partial \phi_j^{(3)}}{\partial x} + \phi_i^{(3)} \frac{\partial \phi_j^{(2)}}{\partial x} \right) + \frac{1+\alpha^2}{\gamma\bar{p}} \bar{u}\phi_i^{(3)} \frac{\partial \phi_j^{(3)}}{\partial x} \right] d\Omega. \end{aligned} \tag{26}$$

The eigenvalues of these matrices can predict the stability of the ROM system. For the symmetry inner product case, and with applying the integral-by-parts rule, (26) becomes

$$\begin{aligned} l_{ij} &= \int_\Omega \left[\bar{\rho}\bar{u}\phi_j^{(1)} \frac{\partial \phi_i^{(1)}}{\partial x} + \phi_j^{(1)} \frac{\partial \phi_i^{(3)}}{\partial x} + \phi_j^{(3)} \frac{\partial \phi_i^{(1)}}{\partial x} + \alpha^2 \bar{\rho}\bar{u}\gamma\bar{p}\phi_j^{(2)} \frac{\partial \phi_i^{(2)}}{\partial x} \right. \\ &\quad \left. + \alpha^2 \bar{\rho}\bar{u} \left(\phi_j^{(2)} \frac{\partial \phi_i^{(3)}}{\partial x} + \phi_j^{(3)} \frac{\partial \phi_i^{(2)}}{\partial x} \right) + \frac{1+\alpha^2}{\gamma\bar{p}} \bar{u}\phi_j^{(3)} \frac{\partial \phi_i^{(3)}}{\partial x} \right] d\Omega \\ &\quad + \left[-\bar{\rho}\bar{u}\phi_i^{(1)}\phi_j^{(1)} - \phi_i^{(1)}\phi_j^{(3)} - \phi_i^{(3)}\phi_j^{(1)} - \alpha^2 \bar{\rho}\bar{u}\gamma\bar{p}\phi_i^{(2)}\phi_j^{(2)} \right. \\ &\quad \left. - \alpha^2 \bar{\rho}\bar{u} \left(\phi_i^{(2)}\phi_j^{(3)} + \phi_i^{(3)}\phi_j^{(2)} \right) - \frac{1+\alpha^2}{\gamma\bar{p}} \bar{u}\phi_i^{(3)}\phi_j^{(3)} \right]_0^{L_X}, \end{aligned} \tag{27}$$

leading to:

$$l_{ij} = -l_{ji} + b_{ij}. \tag{28}$$

So, the matrix $\mathbf{L}$ can be written in matrix form

$$\mathbf{L} = \begin{bmatrix} 0 & l_{12} & l_{13} & \cdots & l_{1M} \\ -l_{12} & 0 & l_{23} & \cdots & l_{2M} \\ -l_{13} & -l_{23} & 0 & \cdots & l_{3M} \\ \vdots & \vdots & \vdots & \ddots & \vdots \\ -l_{1M} & -l_{2M} & -l_{3M} & \cdots & 0 \end{bmatrix} + \begin{bmatrix} \frac{1}{2}b_{11} & 0 & 0 & \cdots & 0 \\ b_{21} & \frac{1}{2}b_{22} & 0 & \cdots & 0 \\ b_{31} & b_{32} & \frac{1}{2}b_{33} & \cdots & 0 \\ \vdots & \vdots & \vdots & \ddots & \vdots \\ b_{1M} & b_{2M} & b_{3M} & \cdots & \frac{1}{2}b_{MM} \end{bmatrix}. \tag{29}$$

Downloaded by Mingjun Wei on February 5, 2016 | http://arc.aiaa.org | DOI: 10.2514/6.2016-1106

The first part in (30) is a skew-symmetric matrix, which always has eigenvalues being pure imaginary numbers (i.e. zero in its real part). The second matrix is a lower triangular matrix, which has eigenvalues on its diagonal entries: $\frac{1}{2}b_{11}$, $\frac{1}{2}b_{22}$, $\frac{1}{2}b_{33}$, ..., $\frac{1}{2}b_{MM}$. If they are all non-positive real numbers, the ordinary differential equations for the reduced order model is stable ($b_{jj} \leq 0$). In general,

$$\begin{aligned} 2b_{jj} \quad = \quad & \left[-\bar{\rho}\bar{u}\left(\phi_j^{(1)}\right)^2 - 2\phi_j^{(1)}\phi_j^{(3)} - \alpha^2\bar{\rho}\bar{u}\gamma\bar{p}\left(\phi_j^{(2)}\right)^2 - 2\alpha^2\bar{\rho}\bar{u}\left(\phi_j^{(2)}\phi_j^{(3)}\right) \right. \\ & \left. -\frac{1+\alpha^2}{\gamma\bar{p}}\bar{u}\left(\phi_j^{(3)}\right)^2 \right]_{(\text{at } L_x)} + \left[\bar{\rho}\bar{u}\left(\phi_j^{(1)}\right)^2 + 2\phi_j^{(1)}\phi_j^{(3)} + \alpha^2\bar{\rho}\bar{u}\gamma\bar{p}\left(\phi_j^{(2)}\right)^2 \right. \\ & \left. +2\alpha^2\bar{\rho}\bar{u}\left(\phi_j^{(2)}\phi_j^{(3)}\right) + \frac{1+\alpha^2}{\gamma\bar{p}}\bar{u}\left(\phi_j^{(3)}\right)^2 \right]_{(\text{at } 0)}. \end{aligned} \tag{30}$$

The above derivation suggests that the stability of ROM using symmetry inner product is general stable but the stability can be altered by different boundary conditions.

IV. Numerical Results and Analysis

Two similar cases are considered here. In the first case, we had $M = 0.5$, $L_x = 20$, and $T_{tot} = 12$ and used 120 snapshots equally spaced in time for POD-Galerkin projection process. In the second case, with other parameters being the same, we ran for a longer time $T_{tot} = 20$, which represents exactly one period (when periodic condition is applied), and 200 snapshots are used. Two types of boundary conditions, periodic and non-reflective, are considered for both cases. More important, we applied different inner products, L^2 and symmetry inner products, in the modeling process to compare the ROM performance in stability, convergency, and accuracy.

IV.A. Stability

For a linear problem, the stability of ROMs is determined by its coefficient matrix, of which all real parts of the eigenvalues need to be non-positive to be stable. ROMs with different number of modes (1 to 32) are examined for stability [18].

IV.A.1. $T_{tot} = 12$

When the total time $T_{tot} = 12$ is shorter than a period (to represent a more "transitional" case), figure 1 compared the stability of ROMs with different boundary conditions with different number of modes.

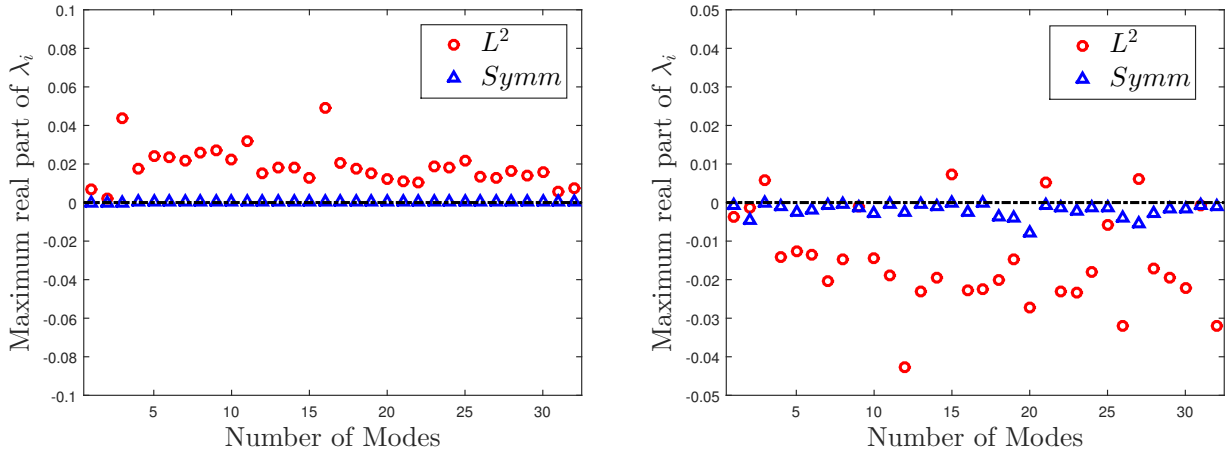

(a) Periodic boundary condition

(b) Non-reflective boundary condition

Figure 1: Maximum real parts of eigenvalues using L^2 and Symmetry inner products with different boundary conditions(T=12).

Downloaded by Mingjun Wei on February 5, 2016 | http://arc.aiaa.org | DOI: 10.2514/6.2016-1106

a) Periodic boundary condition

Figure 1a shows that the real part of eigenvalues are all zeros for symmetry case with periodic boundary conditions. Thus, it matches with the discussion of (31) which shows all zero real part for eigenvalues when b_{jj}'s are zeros (i.e. periodic condition). On the other hand, for ROMs using L^2 inner products, the maximum real parts of the eigenvalues are positive and indicate instability.

b) Non-reflective boundary condition

There are some specific number of mode which L^2 inner product has positive maximum real parts of eigenvalues and ROMs with these number of modes are unstable (figure 1b). On the other hand, ROMs using the symmetry inner product are always stable for all the eigenvalues' real parts being negative.

IV.A.2. $T_{tot} = 20$

When the total time $T_{tot} = 20$ is exactly one period, figure 2 compared the stability of ROMs with different boundary conditions and different number of modes.

Downloaded by Mingjun Wei on February 5, 2016 | http://arc.aiaa.org | DOI: 10.2514/6.2016-1106

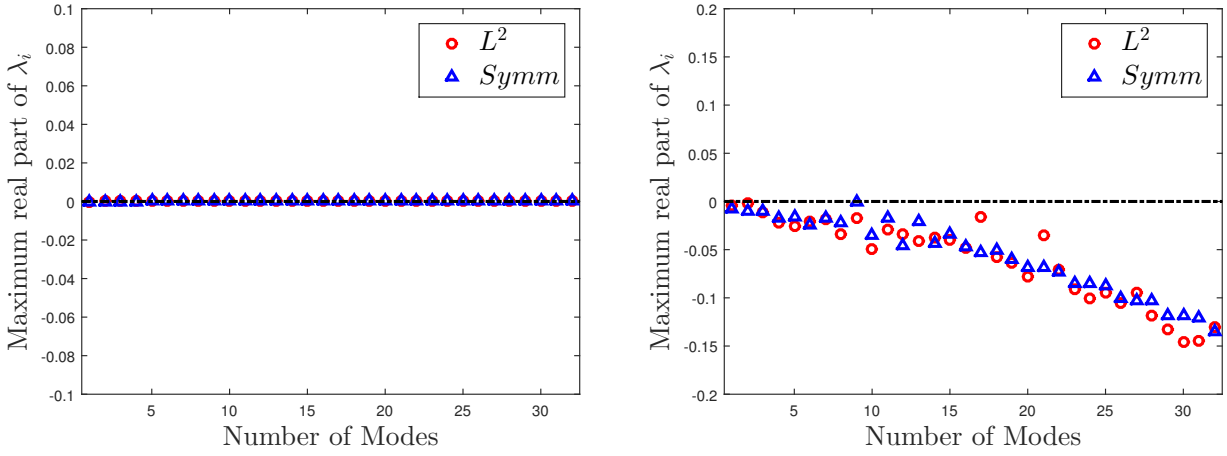

(a) Periodic boundary condition

(b) Non-reflective boundary condition

Figure 2: Maximum real parts of eigenvalues using L^2 and Symmetry inner products with different boundary conditions(T=20).

a) Periodic boundary condition

Non-dimensional time of $T_{tot} = 20$ represents exactly one period (when periodic conditions are applied), and the ROM coefficient matrix is skew-symmetric for both types of inner product. All the eigenvalues are zeros and both ROMs are stable for any number of modes (figure 2a). Because of the same stability behavior, we will focus on this case for later study of convergency and accuracy.

b) Non-reflective boundary condition

For this special case there is neither incoming nor outgoing wave for the left boundary ($x = 0$), It puts the second term in (31) zero for symmetry inner product case. For the right boundary ($x = L_x$), which determines the first term in (31), where most of the sub-terms have negative values which stabilize the system (figure 2b). For the L^2 inner product ROM, for similar reasons, the system is also stable for any number of modes.

IV.B. Convergency

Besides the stability, the convergency of ROMs with the number of modes is another critical feature to consider. In the convergency study, we only considered the cases with periodic condition and the data with one exact period (e.g. $T_{tot} = 20$).

In the comparison, we considered the "energy" captured by each model as an indication for its convergency. Since different definition of inner products also provide different definition of energy as shown in (21) and (24). We need to consider the energy separately by their own definition.

To analyze the quality of the ROMs using different types of inner products or in the other words different types of energy norms, the total energy captured with the ROMs compared with the POD and exact solution's total energy. Figure 3a shows that for L^2 inner product the ROM captures less energy than the energy of the reconstruction of the same number of POD modes. On the other hand, figure 3b shows that the symmetry inner product model is more "energy efficient" and captures even more energy than the reconstruction of POD modes.

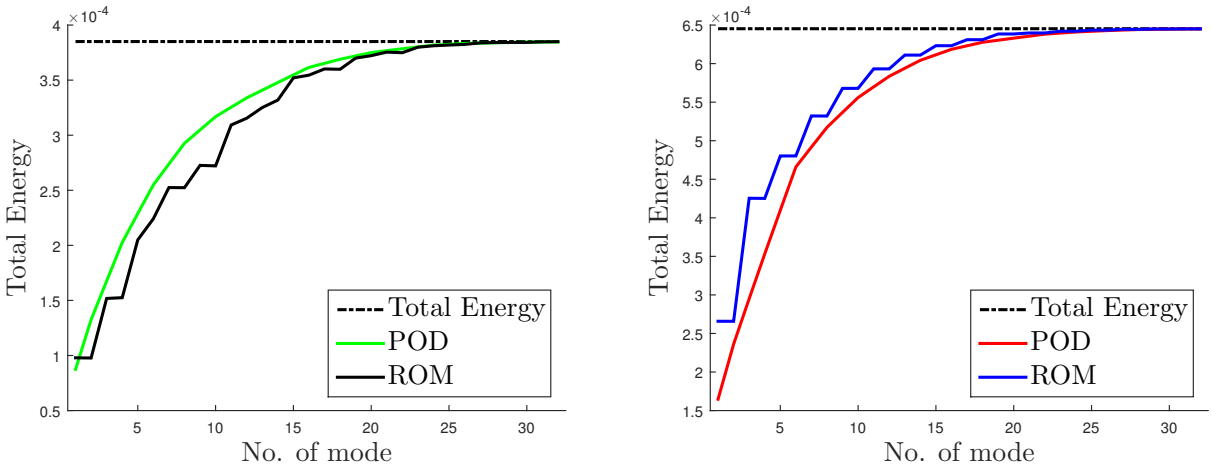

(a) L^2 inner product

(b) Symmetry inner product

Figure 3: Energy calculation for different number of modes using different inner products.

IV.C. Mode Coefficients Accuracy

The final comparison is the accuracy of mode coefficients computed by ROMs built from the same number of modes but different inner products, L^2 and symmetry, are used in the process.

In figures 4 and 5, we compared the temporal coefficients of modes, in forms of phase portrait, for the ROMs built with respectively 8 and 16 modes. In both figures, we use the phase portraits of a_1 versus a_2, and a_2 versus a_4 to show two different types of attractors. Here, we noticed that the ROM using symmetry inner product only needs 8 modes to match perfectly with the exact solution, while the model using traditional L^2 inner product needs 16 modes to match well with the exact solution. The phase portraits from symmetrical ROM also depict a cleaner picture of dynamics for attractors, which by itself is usually an indication of better representation of underline dynamics.

Downloaded by Mingjun Wei on February 5, 2016 | http://arc.aiaa.org | DOI: 10.2514/6.2016-1106

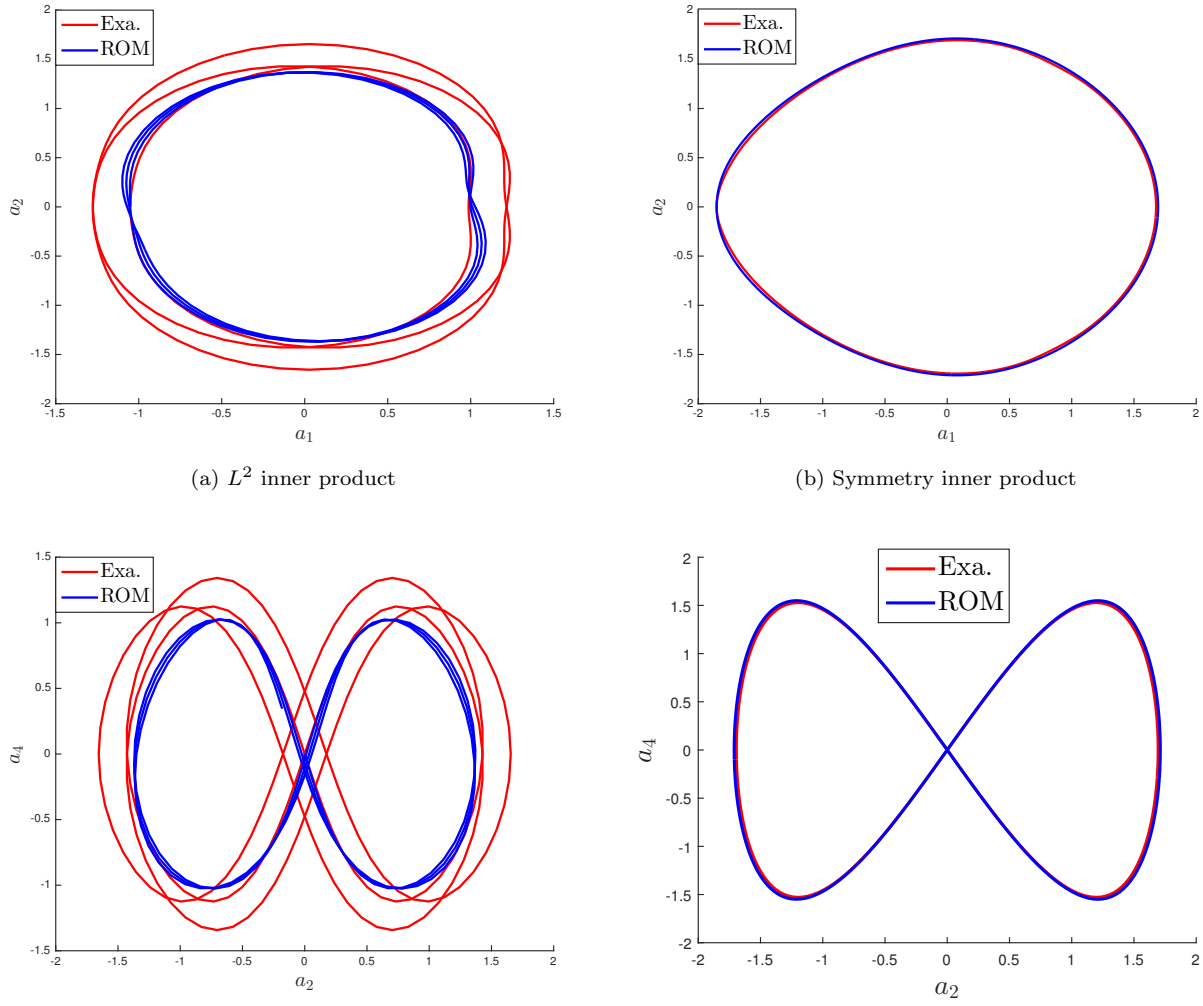

(a) L^2 inner product

(b) Symmetry inner product

(c) L^2 inner product

(d) Symmetry inner product

Figure 4: Phase portraits of mode coefficients computed by 8-mode ROMs using L^2 and Symmetry inner products.

Downloaded by Mingjun Wei on February 5, 2016 | http://arc.aiaa.org | DOI: 10.2514/6.2016-1106

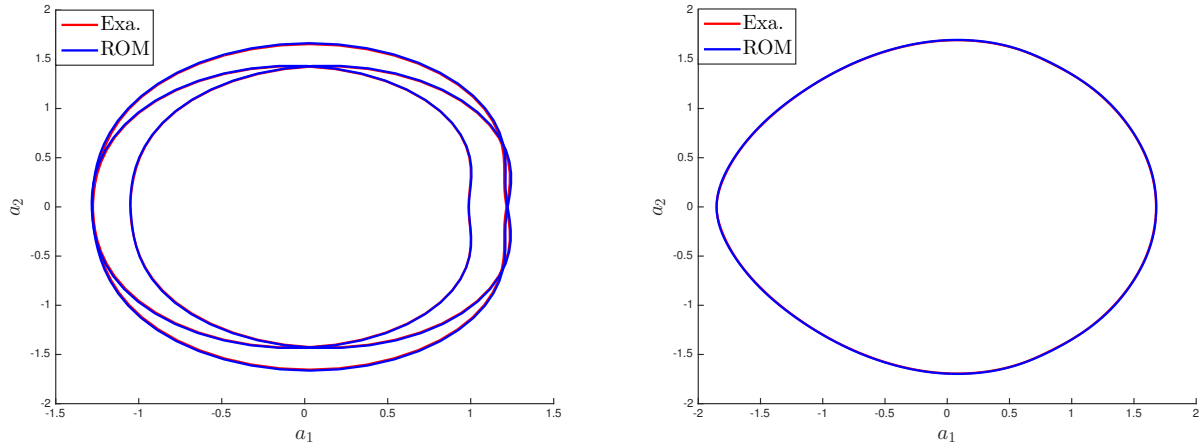

(a) L^2 inner product

(b) Symmetry inner product

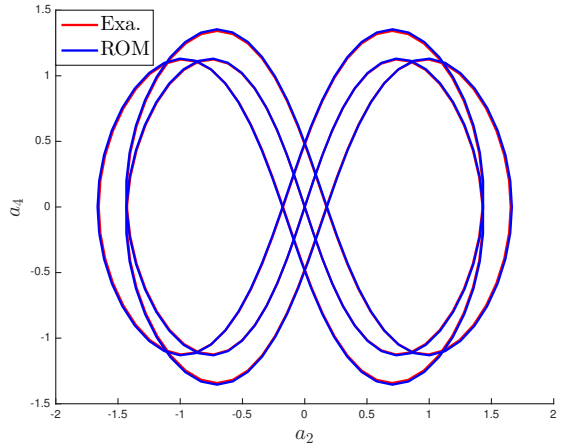

(c) L^2 inner product

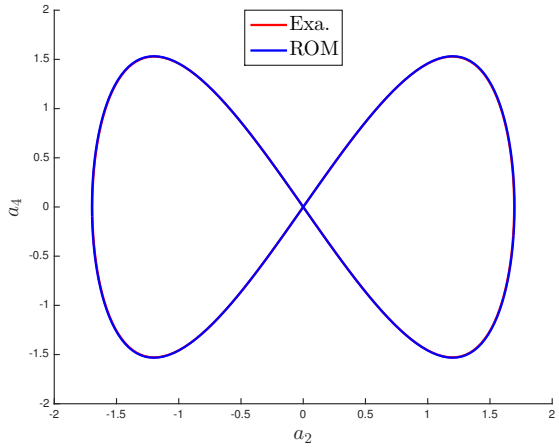

(d) Symmetry inner product

Figure 5: Phase portraits of mode coefficients computed by 16-mode ROMs using L^2 and Symmetry inner products.

V. Conclusion and Discussion

We used two different definition of inner products, the traditional L^2 inner product and a specially designed symmetry inner product, to derived POD-Galerkin models for a linearized Euler equation. A simple derivation of coefficients matrix for the resulted ROM using symmetry inner product suggests a universally stable solution for periodic boundary conditions, thus is not the case for the ROM using L^2 inner product. Further analysis of general boundary conditions beside the periodic one suggests that the stability may stay in most of cases for a symmetrical ROM.

In our test case using an exact solution for a traveling wave, we noticed that the L^2 based ROM, not surprisingly, captures less energy than the theoretical upper bound, which is the energy in the reconstructed flow by the same number of POD modes; however, the symmetrical ROM can even capture more energy surpassing such theoretical upper bound.

Using the same test case, we also compared the accuracy of ROMs by a comparison of phase portraits of mode coefficients computed directly from these ROMs. A direct projection of exact solutions to the same POD mode provides an exact solution to compare to. In this study, we found that the ROM using symmetry inner product shows superior accuracy and the results can match perfectly with the exact solution for a 8-mode ROM. On the other hand, the ROM using L^2 inner product needs at least 16 modes to to reach

Downloaded by Mingjun Wei on February 5, 2016 | http://arc.aiaa.org | DOI: 10.2514/6.2016-1106

the same accuracy. It is interesting to notice that the attractors, represented by phase portraits, from the symmetrical ROM, depicts a more organized picture and therefore a cleaner representation of underline dynamics.

VI. Acknowledgment

The authors gratefully acknowledge the support from Army Research Lab (ARL) through Army High Performance Computing Research Center (AHPCRC) and Micro Autonomous Systems and Technology (MAST) CTA. The authors also acknowledge Dr. Matthew Barone for all the help and fruitful discussion.

References

[1]Woon, S. and Marshall, S., "Design of multivariable control systems using reduced-order models," *Electronics Letters*, Vol. 11, No. 15, July 1975, pp. 341–342.

[2]Lall, S., Marsden, J. E., and Glavaški, S., "A subspace approach to balanced truncation for model reduction of nonlinear control systems," *Int. J. Robust Nonlinear Control*, Vol. 12, 2002, pp. 519–535.

[3]Bergmann, M., Cordier, L., and Brancher, J.-P., "Optimal rotary control of the cylinder wake using proper orthogonal decomposition reduced-order model," *Physics of fluids*, Vol. 17, No. 9, 2005, pp. 097101–097101.

[4]Rowley, C. W. and Williams, D. R., "Dynamics and control of high-Reynolds-number Flow over open cavities," *Ann. Rev. Fluid Mech.*, Vol. 38, 2006, pp. 251–276.

[5]Michopoulos, J., Tsompanopoulou, P., Houstis, E., Rice, J., Farhat, C., Lesoinne, M., and Lechenault, F., "DDEMA: A Data Driven Environment for Multiphysics Applications," *Computational Science ICCS 2003*, edited by P. Sloot, D. Abramson, A. Bogdanov, Y. Gorbachev, J. Dongarra, and A. Zomaya, Vol. 2660 of *Lecture Notes in Computer Science*, Springer Berlin Heidelberg, 2003, pp. 309–318.

[6]Cortial, J., Farhat, C., Guibas, L., and Rajashekhar, M., "Compressed Sensing and Time-Parallel Reduced-Order Modeling for Structural Health Monitoring Using a DDDAS," *Computational Science ICCS 2007*, edited by Y. Shi, G. van Albada, J. Dongarra, and P. Sloot, Vol. 4487 of *Lecture Notes in Computer Science*, Springer Berlin Heidelberg, 2007, pp. 1171–1179.

[7]Rowley, C. W. and Marsden, J. E., "Reconstruction Equations and the Karhunen-Loève Expansion for Systems with Symmetry," *Phys. D*, Vol. 142, 2000, pp. 1–19.

[8]Rowley, C. W., Kevrekidis, I. G., Marsden, J. E., and Lust, K., "Reduction and reconstruction for self-similar dynamical systems," *Nonlinearity*, Vol. 16, 2003, pp. 1257–1275.

[9]Rowley, C. W., Colonius, T., and Murray, R. M., "Model reduction for compressible flow using POD and Galerkin projection," *Phys. D*, Vol. 189, No. 1–2, Feb. 2004, pp. 115–129.

[10]Wei, M. and Rowley, C. W., "Low-dimensional models of a temporally evolving free shear layer," *J. Fluid Mech.*, Vol. 618, 2009, pp. 113–134.

[11]Wei, M., Qawasmeh, B. R., Barone, M., van Bloemen Waanders, B. G., and Zhou, L., "Low-dimensional model of spatial shear layers," *Physics of Fluids*, Vol. 24, No. 1, 2012, pp. 014108.

[12]Qawasmeh, B. R. and Wei, M., "Low-dimensional models for compressible temporally developing shear layers," *Journal of Fluid Mechanics*, Vol. 731, 9 2013, pp. 364–393.

[13]Noack, B. R., Afanasiev, K., Morzynski, M., Tadmor, G., and Thiele, F., "A hierarchy of low-dimensional models for the transient and post-transient cylinder wake," *Journal of Fluid Mechanics*, Vol. 497, No. 1, 2003, pp. 335–363.

[14]Berkooz, G., Holmes, P., and Lumley, J. L., "The proper orthogonal decomposition in the analysis of turbulent flows," *Ann. Rev. Fluid Mech.*, Vol. 25, 1993, pp. 539–575.

[15]Holmes, P., Lumley, J. L., and Berkooz, G., *Turbulence, Coherent Structures, Dynamical Systems and Symmetry*, Cambridge University Press, Cambridge, 1996.

[16]Colonius, T., Rowley, C. W., Freund, J. B., and Murray, R. M., "On the choice of norm for modeling compressible flow dynamics at reduced-order using the POD," IEEE 2002 Conference on Decision and Control, Las Vegas, NV, 2002.

[17]Gustafsson, B. and Sundstrom, A., "Incompletely Parabolic Problems in Fluid Dynamics," *SIAM Journal on Applied Mathematics*, Vol. 35, No. 2, 1978, pp. pp. 343–357.

[18]Barone, M. F., Kalashnikova, I., Segalman, D. J., and Thornquist, H. K., "Stable Galerkin reduced order models for linearized compressible flow," *Journal of Computational Physics*, Vol. 228, No. 6, 2009, pp. 1932 – 1946.

[19]Sirovich, L., "Turbulence and the dynamics of coherent structures. I - Coherent structures. II - Symmetries and transformations. III - Dynamics and scaling," *Quarterly of Applied Mathematics*, Vol. 45, Oct. 1987, pp. 561–571.

[20]D.M. Luchtenburg, B. N. . M. S., "An introduction to the POD Galerkin method for fluid flows with analytical examples and MATLAB source codes," Tech. rep., Berlin Institute of Technology, Germany, 01 2009.

Downloaded by Mingjun Wei on February 5, 2016 | http://arc.aiaa.org | DOI: 10.2514/6.2016-1106